Proceedings of the 37th IAHR World Congress
August 13 – 18, 2017, Kuala Lumpur, Malaysia

FREE-SURFACE AND VELOCITY CHARACTERISTICS OF TIDAL BORE PROPAGATION AGAINST A SLOPE: EXPERIMENTS ON DECELERATING BORES

YOUKAI LI(1) & HUBERT CHANSON(2)

(1) The University of Queensland, School of Civil Engineering, Brisbane QLD 4072, Australia,
youkai.li@uq.net.au; h.chanson@uq.edu.au

ABSTRACT

A tidal bore is a hydraulic jump in translation occurring in the estuarine zone where the river has a funnel-shaped mouth. For a decelerating bore propagating upstream against a steep slope, its properties vary at different locations before it finally changes into an arrested bore: i.e. a stationary hydraulic jump. The present study conducted some novel and systematic research on the transformation of a decelerating bore into a stationary hydraulic jump in a relatively large channel with adverse slope. The arrested bore could be of different types: an undular jump with long shock waves, strong secondary waves and no breaking, a partially breaking jump with long shock waves and strong secondary waves, or a strongly breaking jump with short shock waves and weak secondary waves. All the experiments were repeated more than 25 times to yield some ensemble-averaged results in terms of the free-surface characteristics, velocity and turbulent Reynolds stresses. Physically, the decelerating bore propagation induced maximum free-surface and velocity fluctuations associated with the bore front passage, but there was a time lag between the occurrence of the maximum fluctuations, hinting some coupling effect between the free-surface elevations and turbulent velocity during the decelerating bore passage.

Keywords: Decelerating bores; physical modeling; arrested hydraulic jump; ensemble-averaging.

1 INTRODUCTION

A tidal bore is a positive surge of tidal origin, occurring in an estuary where the river has a funnel-shaped mouth, a large tidal range and low fresh water discharge (Chanson, 2011a; Lighthill, 1978). The bore is a hydrodynamic shock, sometimes called a hydraulic jump in translation (Henderson, 1966) (Figure 1). Field observations showed that tidal bores could highly enhance the turbulent process in estuaries inducing strong upward convection of riverbed materials and upstream advection of suspended sediments (Keevil et al., 2015; Chanson et al., 2011). The shape of the bore front is characterized by its Froude number, Fr_1, defined in a rectangular channel as:

$$Fr_1 = \frac{V_1 + U}{\sqrt{g \times d_1}} \quad [1]$$

where d_1 and V_1 are respectively the upstream initial flow depth and velocity immediately prior to the tidal bore passage, U is the bore celerity positive upstream and g is the gravity acceleration. The Froude number, Fr_1 is always greater than unity (Liggett, 1994; Henderson, 1966). For a tidal bore with Froude number slightly larger than unity, between 1 and 1.2-1.3, an undular bore is seen, characterised by a smooth rise of the free-surface, followed by a train of strong secondary free-surface undulations (Koch and Chanson, 2008; Treske, 1994) (Figure 1, Right). A tidal bore with Froude number between 1.2-1.3 and 1.5-1.8 is a breaking bore with weak secondary waves behind the bore front. When the bore Froude number is larger than 1.5-1.8, a breaking bore takes place: the bore front is characterised by an abrupt roller with air entrainment and highly turbulent motion (Leng and Chanson, 2015; Chanson, 2010) (Figure 1, Left).

When a tidal bore propagates upstream against a steep adverse slope, the bore may lose its celerity and transform into a stationary hydraulic jump. During the transformation process, the properties of the tidal bore slowly changes and may cause some erosion and scouring to the riverbed (MacDonald et al., 2009; Bellal et al., 2003). The formation of a bore propagating against a steep mobile-bed slope, its deceleration and vanishing may also be associated with a cyclic behaviour (Parker and Izumi, 2000; Grant, 1997; Parker, 1996). Pertinent studies included Chanson (2011b), MacDonald et al. (2009) and Carling (1995).

The deceleration of a tidal bore has yet been rarely studied to date. The experiments of Chanson (2011b) highlighted the complicated and slow transformation of a moving bore into a stationary hydraulic jump on an adverse steep slope. The present study aims to expand the work by conducting systematic laboratory experiments of the transformation of tidal bores into stationary hydraulic jumps for a broader range of flow conditions.

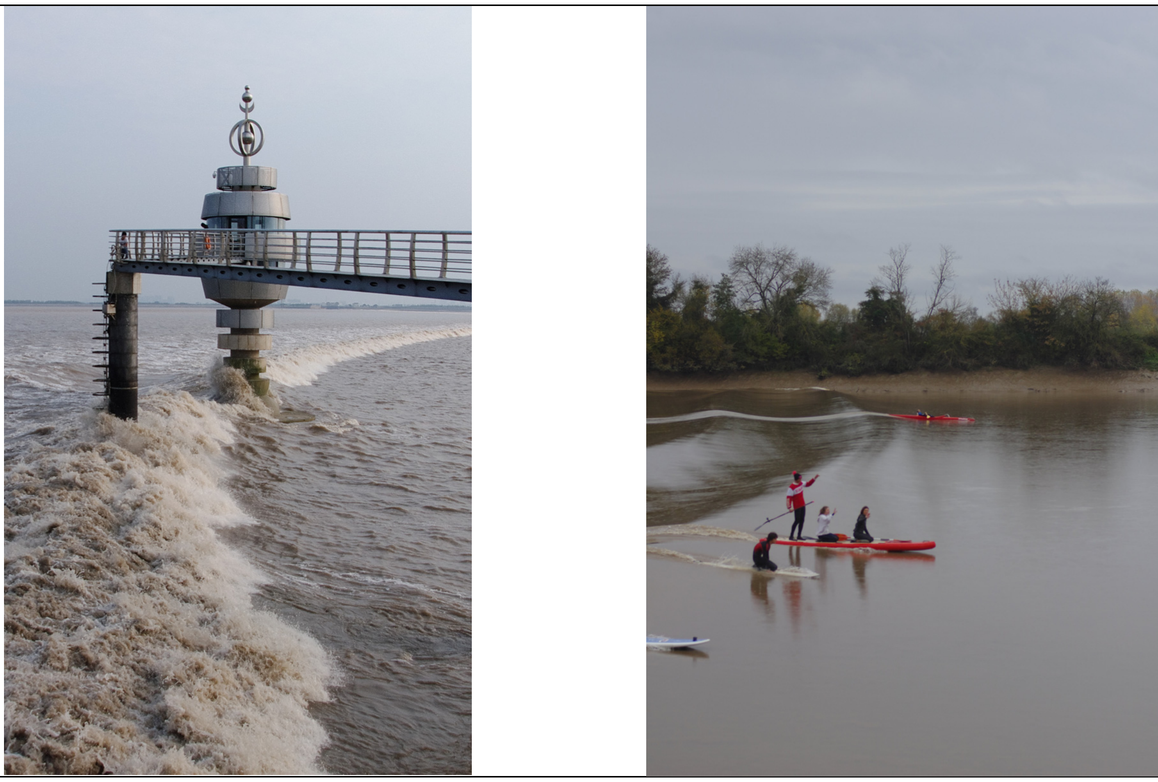

Figure 1. Photographs of tidal bores - Left: breaking tidal bore of the Qiantang River at Yanguan (China) on 23 September 2016; Right: undular tidal bore of the Dordogne River between Luchey and Port de Moulon (France) on 12 November 2016.

2 EXPERIMENTAL FACILITY, INSTRUMENTATION AND FLOW CONDITIONS

2.1 Facility and instrumentation

New experiments were conducted in a large tilting rectangular flume at the University of Queensland, Australia. The channel was 15 m long, 0.495 m wide and 0.465 m high. The channel bed was made of smooth PVC and the sidewalls were made of glass (Figure 2A). A constant head reservoir supplied the water to an upstream intake tank (1.43m×1.24m×1.0m), equipped with baffles and flow straighteners and connected to the start of the glass-walled channel by a smooth convergent section, enabling a quasi-uniform low-turbulence inflow into the glass-walled test section. The water discharge, Q was measured by a Venturi meter mounted in the water supply, designed based upon British Standard (British Standard, 1943) and calibrated on site with an error of less than 2%. The bed slope, $S_o = \sin\theta$, with θ, the angle between channel bed and the horizontal, could be finely adjusted by a mechanical screw jack system, with an estimated error of less than 1×10^{-4}.

A fast-closing Tainter gate was located at $x = x_{gate} = 14.17$ m, with x the longitudinal distance from the start of the glass-walled test section, leaving an opening h between the lower gate edge and invert (Figure 2B). At the location of the Tainter gate, the initial water surface was typically lower than h. The bore was initially generated using a temporary manually-controlled fast-closing adjunctive gate: it was shut down in less than 0.2 s, kept partially closed for 3-4 s and lifted up in less than 0.2 s.

The steady flow depths were measured using a pointer gauge. Measurements of unsteady water elevations were performed with 6 acoustic displacement meters (ADMs) Microsonic™ Mic+25/IU/TC, mounted above the channel centreline at x = 14.26 m (immediately downstream of Tainter gate), 13.85 m (immediately upstream of Tainter gate), 9.10 m, 8.10 m, 7.00 m and 6.10 m. All ADMs were sampled at 200 Hz. The water velocities were recorded by a Nortek™ Vectrino+ acoustic Doppler velocimeter (ADV) equipped with a side-looking probe (Probe ID: VCN 7999). The ADV control volume was located at x = 7.00 m on the channel centreline. The velocity range was ±2.5 m/s and the sampling rate was 200 Hz. The accuracy was ±0.5% of the velocity range. The vertical elevation of the ADV probe was controlled by a fine adjustment traverse mechanism connected to a Hafco™ M733 digimatic vertical scale unit. The error of the vertical position of the ADV probe was less than 0.025 mm. The accuracy of the longitudinal position along the channel was ±2 mm while the error of the transverse position was ±1 mm.

  / ISSN 1562-6865 (Online) - ISSN 1063-7710 (Print)

Two cameras were used to track the decelerating bore propagation against the steep slope. A dSLR camera Canon™ EOS 1200D (25fps; resolution: 640×480p) was placed at x=13.0 m on a tripod to record the tidal bore for a relatively short time span after its generation. The time origin was detected by the sound of gate closure. A camcorder Sony™ HDR-XR160 (25fps, 1400×1080p) followed the decelerating bore from the generation up to its transformation into a stationary hydraulic jump. For each flow condition, video recording was also performed at the final bore locations to track the oscillations of the arrested bore.

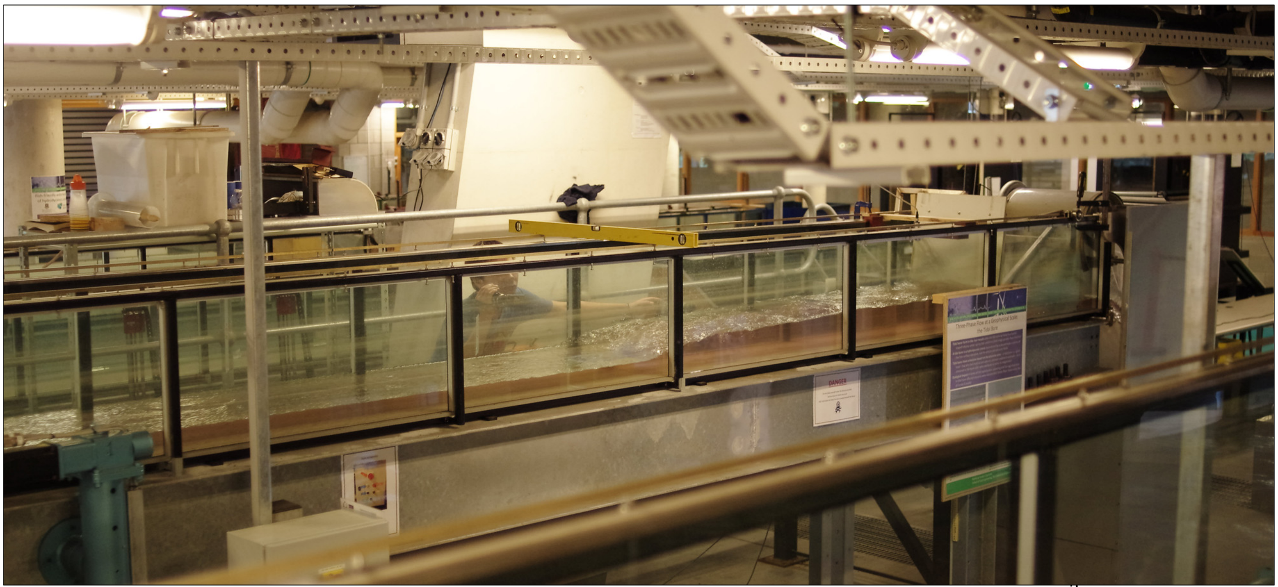

(A) Experimental channel - Initial bore propagation shortly after gate closure - Q = 0.039 m^3/s, d_1 = 0.065 m, S_o = 0.0068 - Red arrow points to bore front, bore propagation from right to left.

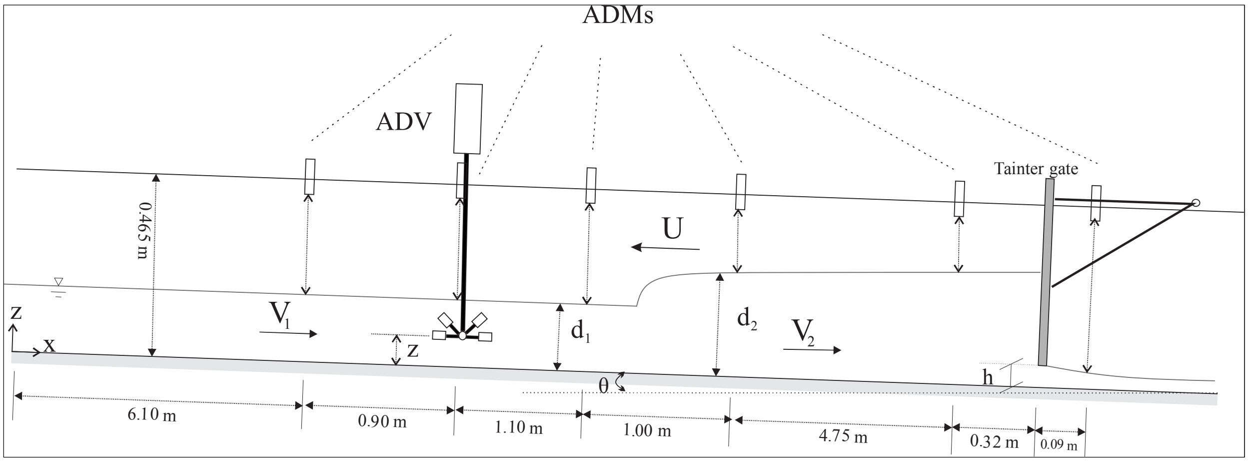

(B) Schematic diagram of the experimental channel facility and instrumentation setup (not to scale) - At x = 7.00 m, the ADM was immediately above the ADV control volume.

Figure 2. Experimental facility of decelerating bore investigation at the University of Queensland.

2.2 Experimental flow conditions

Two initial flow rates Q = 0.039 and 0.061 m^3/s and two bed slopes S_o = 0.0068 and 0.0110 were selected, following a series of preliminary tests to ensure that the bore front was arrested between x = 0 m and x= 6.10 m. Table 1 lists the experimental flow conditions, where the initial flow depth, d_1, the bore celerity, U, the initially-steady supercritical flow Froude number, Fr_o and the bore Froude number, Fr_1 were observed at x = 7.00 m, and x_s is the position of the bore front. In Table 1, only the final position of the arrested bore is shown, and B is the channel width.

The velocity profiles in the initially steady flow on the tilted bed showed the presence of a developing boundary layer. In the developing turbulent boundary layer, the longitudinal velocity component distribution followed a 1/8th power law. For all flow conditions, the initial flow was partially developed at x = 7.00 m (ADV sampling location). Using the von Karman momentum integral equation, the boundary shear stress was estimated to be τ_o = 1.2-1.8 Pa at x =7.00 m for all experiments.

For all experiments, the instrumentations started recording the initially steady flow conditions for 60 s before the bore generation. The data acquisition stopped after the bore became arrested. Each series of experiments was repeated more than 25 times to perform some ensemble-average analysis following Leng and Chanson (2016) as well as Chanson and Docherty (2012).

Table 1. Decelerating bore experiments (d_1, U, Fr_o, Fr_1 are flow conditions at x = 7.0m).

Reference	Q (m^3/s)	S_o	d_1 (m)	U (m/s)	Fr_o	Fr_1	x_s (Final) (m)	Remarks
Present study	0.039	0.0110	0.059	0.037	1.76	1.79	3.55	B = 0.495 m Smooth PVC bed
		0.0068	0.066	0.037	1.47	1.52	4.60	
	0.061	0.0110	0.074	0.019	1.95	1.96	5.15	
		0.0068	0.085	0.039	1.59	1.62	3.45	
Chanson (2011b)	0.035 to 0.06	0.009 to 0.027	0.040 to 0.072	0.002 to 0.22	--	1.71 to 2.83	--	B = 0.50 m smooth PVC bed

3 FLOW PATTERNS

3.1 Presentation

Visual, photographic and video observations were carried out to document the basic flow patterns of decelerating bores against the adverse slope. Immediately after gate closure, the bore was breaking for all investigated flow conditions (Table 1). The breaking bore process was characterised by a marked turbulent roller with some air bubble entrainment region following the bore font (Figure 2A).

As a bore propagated upstream against the steep slope, its properties slowly varied, and the bore Froude number decreased with increasing distance from the gate. For comparison, preliminary experiments in the same channel with the same flow rate and a horizontal slope (S_o = 0) showed little changes in bore characteristics along the 15m long flume, as shown by Yeow et al. (2016). As the bore decelerated, its shape evolved with time depending upon the initial flow and new boundary conditions. The bore could remain strongly breaking up to bore arrest. For other flow conditions, the arrested bore could be an undular jump with long shock waves, strong secondary waves and no breaking, or a partially breaking jump with long shock waves and strong secondary waves.

3.2 Bore celerity

The decelerating bore propagations were tracked, yielding the bore front arrival time at different longitudinal locations and the corresponding bore celerities. Figure 3 shows typical dimensionless bore celerity U/V_c data as a function of the dimensionless distance from the Tainter gate $(x_{gate}-x)/x_{gate}$, where V_c is the initially steady critical flow velocity. Their corresponding dimensionless bore locations are shown in Figure 3B, where d_c is the initially steady critical flow depth. In Figure 3, g is the gravity acceleration, and B is the channel width (B = 0.495 m). All tidal bores were arrested before they reached the upstream intake structure, as shown by the vertical line in Figure 3.

Immediately after the gate closure, the newly generated bore grew quasi-instantly, reached a maximum celerity at a short distance from the gate and then propagated further upstream with a decreasing celerity (Figure 3A). The bore celerity decreased rapidly to less than half the initial value, as the result of a combination of both adverse channel slope, adjunctive gate removal and boundary friction. For each flow condition, the fluctuations in decelerating bore arrival times became larger between different repeats at the locations farther away from the Tainter gate (Figure 3B). The whole transformation from a decelerating bore to a stationary hydraulic jump took about 350-450 s. In comparison, the bore took less than 20 s to travel through the whole horizontal channel length, for the same initial flow rate. Compared to the tidal bore propagation in a horizontal channel (S_o = 0), the transformation of a decelerating bore was a much slower process, as discussed by Chanson (2011b), who observed a tidal bore transformation into a stationary hydraulic jump in 300-600 s in a 12 m long 0.5 m wide channel. The entire process would take longer at full scale in a natural river flow condition and the duration should be scaled up according to a Froude similitude.

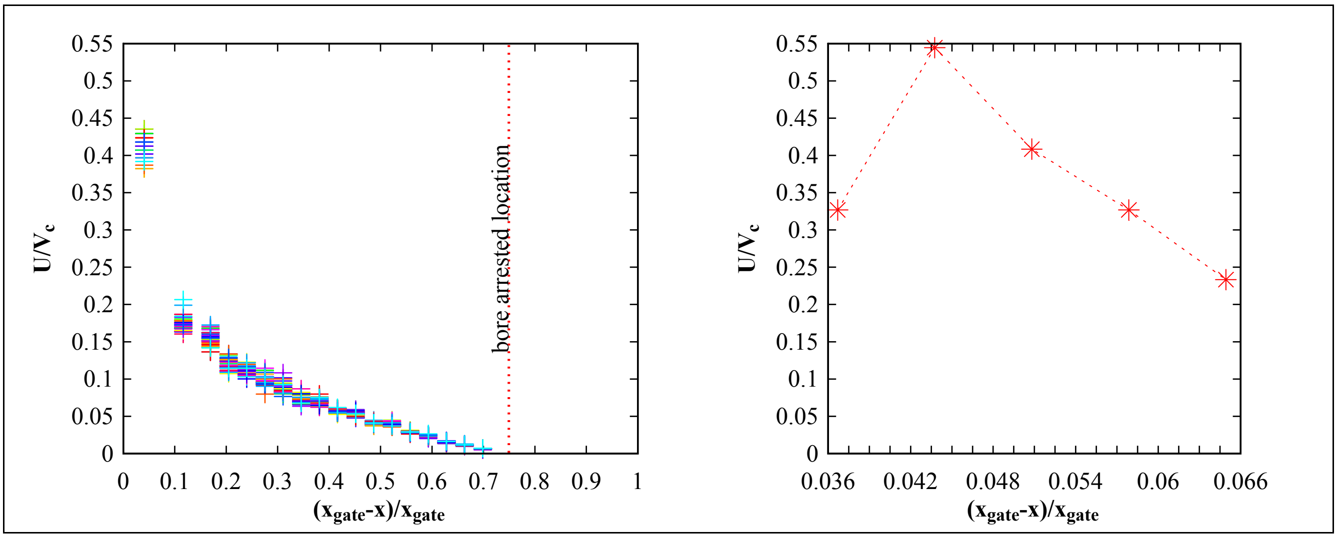

(A) Longitudinal variation in bore celerity - Inset (Right): bore celerity immediately after gate closure.

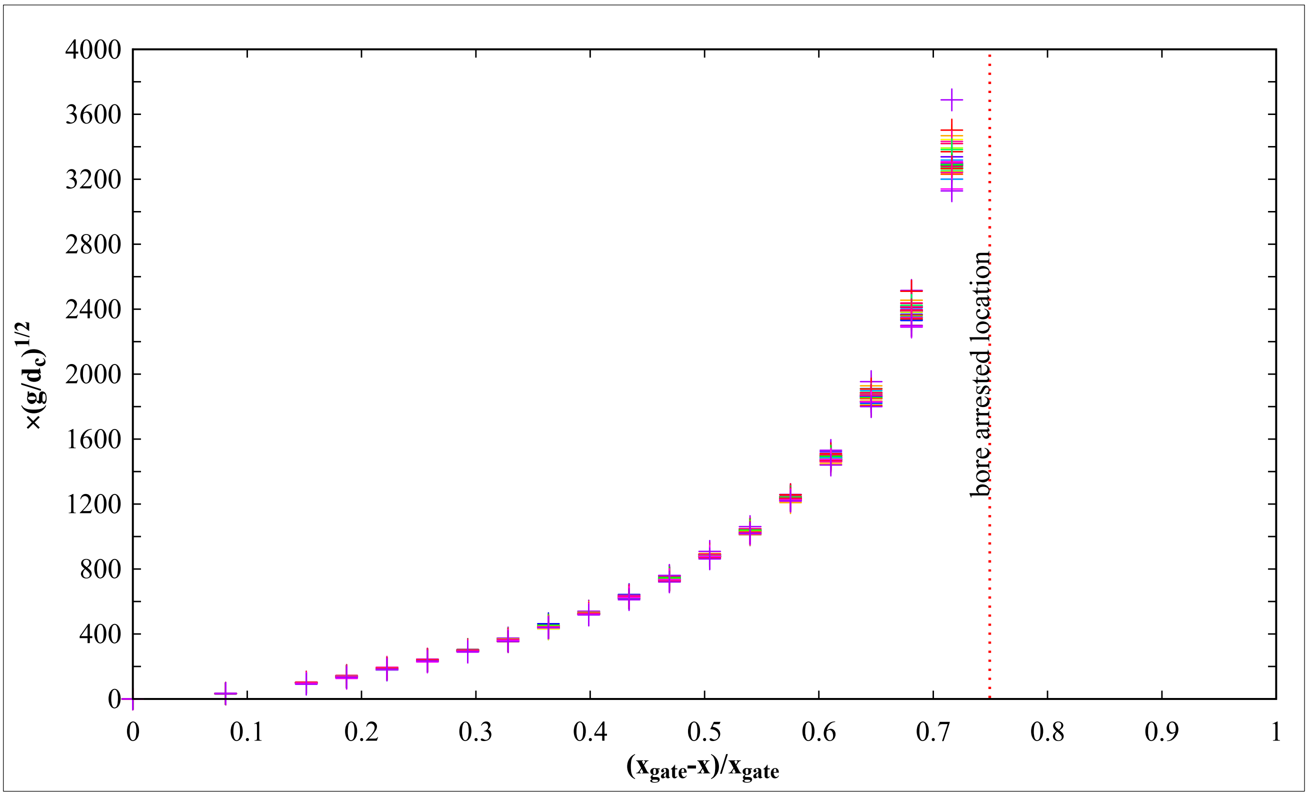

(B) Time-variation of the bore front location x_s.

Figure 3. Propagation characteristics of a decelerating bore. Ensemble-average results - Flow condition: Q = 0.039 m^3/s, S_o = 0.0110, h = 0.065 m, Fr_1 = 1.79 at x = 7.00 m; x_{gate} = 14.17 m, $(x_s)_{final}$ = 3.55 m, d_c = 0.086 m, V_c= 0.9172 m/s.

3.3 Free-surface properties

As the tidal bore is a highly unsteady and turbulent process, a time-average method is not applicable to analyze the free-surface characteristics during the bore passage. A series of ensemble-average measurements were performed for all four flow conditions. For each flow condition, the experiment was repeated more than 25 times on the same day. The median free-surface elevation d_{50} and the difference between the third and first quartiles (d_{75}-d_{25}) were derived from the experimental data. The difference between the third and first quartiles (d_{75}-d_{25}) characterised the instantaneous free-surface fluctuations. Typical results are presented in Figure 4. Herein, the time t = 0 corresponded to the gate closure.

For x > 6.10 m, the decelerating bores all propagated as breaking bores. The passage of the roller was associated with the abrupt increase in the water surface. A train of secondary waves followed the bore front and the water depth after bore passage kept slowly rising because of the backwater effect induced by the closed Tainter gate opening at the downstream end of the channel. For the experiment with the smaller slope (S_o = 0.0068), the well-marked secondary waves developed with time. With both small and large slopes, the secondary wave periods became longer with time at a fixed location. The bore passage was also associated with large free-surface fluctuations (d_{75}-d_{25}), which reached maximum values shortly after the bore roller toe passage (Figure 4).

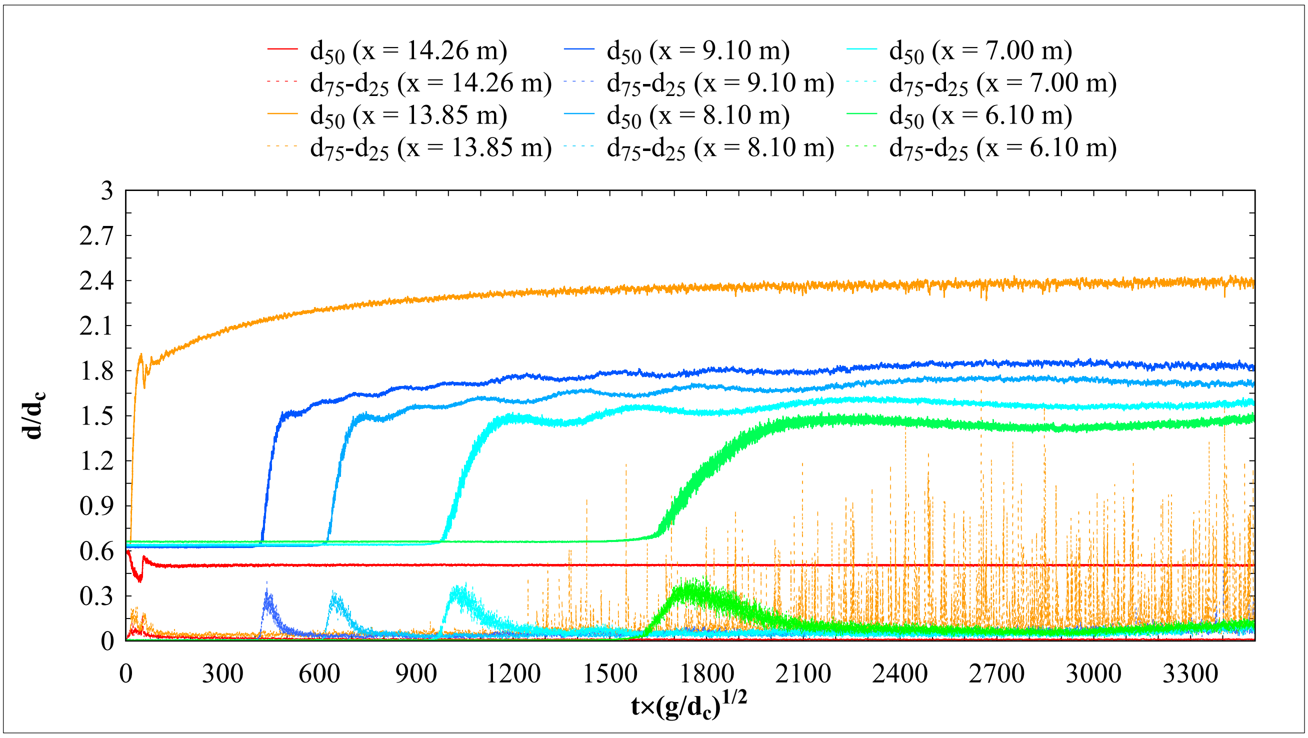

Figure 4. Time-evolutions of ensemble-averaged median free-surface elevations d_{50} and free-surface fluctuations (d_{75}-d_{25}) at different longitudinal locations along the channel - Experimental flow conditions: 32 runs, Q = 0.061 m^3/s, S_o = 0.0110, h = 0.100 m, Fr_1 = 1.96; d_c = 0.116 m.

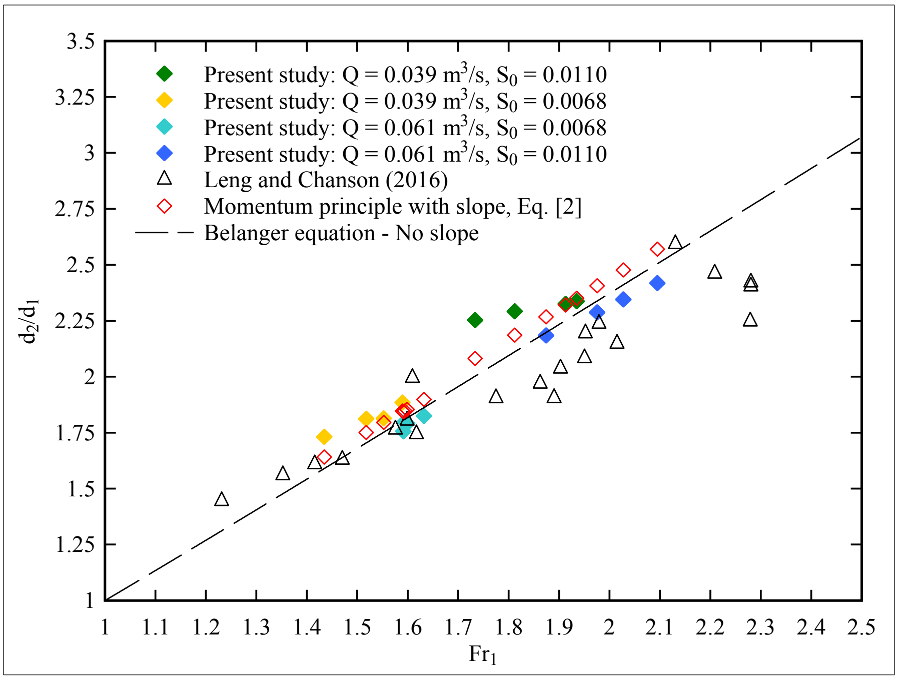

Figure 5. Dimensionless conjugate depth d_2/d_1 as a function of local bore Froude number Fr_1 - Comparison with horizontal slope data (Leng and Chanson, 2016), the momentum principle (Eq. [2]) and the Bélanger equation.

For a smooth rectangular channel, the application of the equations of conservation of mass and momentum in their integral form gives an analytical solution of the conjugate flow properties, namely the ratio of conjugate depth as a function of the Froude number and bed slope (Chanson, 2012). It yields:

$$\frac{d_2}{d_1} = \frac{1}{2} \times \left(\sqrt{(1-\varepsilon)^2 + 8 \times \frac{Fr_1^2}{1-\varepsilon}} - (1-\varepsilon) \right) \qquad [2]$$

where d_1 and d_2 are initial and conjugate flow depths, respectively, and ε is a dimensionless coefficient defined as:

$$\varepsilon = \frac{Vol \times S_o}{B \times d_1^2 \times (Fr_1^2 - 1)} \qquad [3]$$

with B, the channel width and Vol, the control volume encompassing the bore front, such as for weight force, W = ρ×g×Vol. Eq. [2] implies that the ratio of conjugate depths increases with increasing bed slope for a given Froude number. For a smooth horizontal rectangular prismatic channel, Eq. [2] yields to the classical Bélanger equation.

Eq. [2] is compared to the experimental results in Figure 5, as well as to the Bélanger equation and laboratory data in a smooth horizontal channel (Leng and Chanson, 2016). All the data showed a monotonic increase in conjugate depth ratio with increasing Froude number. Since S_o << 1 in the present experiments, the slope effect was small. For a given flow rate, a larger bed slope would yield both larger bore Froude number and larger conjugate depth ratio d_2/d_1 within the experimental flow conditions

4 VELOCITY MEASUREMENTS

Unsteady water velocity measurements during decelerating bores were conducted at the longitudinal location x = 7.00 m. The output data were the longitudinal, transverse and vertical velocity components: V_x, V_y and V_z. Here, V_x is parallel to the channel bed and positive downstream; V_y is parallel to the horizontal and positive towards left sidewall; V_z is normal to the channel bed and positive upwards. Figure 6 presents typical results of ensemble-average analysis. For all the flow conditions, the bore Froude number Fr_1 was larger than 1.5 at x = 7.00 m and the decelerating bores had a breaking roller on the channel centreline. With the passages of the bore front, the longitudinal velocity, V_x presented a marked deceleration by around 50% of the initially steady flow velocity (Figure 6A). The vertical velocity component, V_z had some slight perturbation associated with the bore front passage, although not as strong as the longitudinal velocity deceleration. Since the bore celerity, U only had an amplitude of 0.02 to 0.04 m/s at x = 7.00 m, the deceleration rate was much slower than that of a breaking bore in horizontal channel (Leng and Chanson, 2016; Koch and Chanson, 2009). The longitudinal velocity components always remained positive during the whole process. No velocity reversal was observed, contrarily to observations on a horizontal slope (Koch and Chanson, 2009). The finding was consistent with the instantaneous velocity measurements by Chanson (2011b) in a decelerating bore.

For all flow conditions, V_y and V_z had a mean value of zero, before the decelerating bore arrived at x = 7.00 m (Figure 6B and 6C). The longitudinal flow velocity component, V_x presented sharp decrease at all vertical elevations during the bore front passage. At the same time, the vertical flow component, V_z experienced some initial increase during the bore front passage and then some decrease after the bore crest passage. All the ensemble-averaged velocity components V_x, V_y and V_z presented an oscillating trend linked to the free-surface curvature induced by the secondary waves, especially for decelerating bores with the smallest Froude numbers. These characteristics were similar to the undular bore experiments in a horizontal channel by Leng and Chanson (2016) and Koch and Chanson (2008), as well as the stationary undular hydraulic jump experiments of Lennon and Hill (2006) and Chanson and Montes (1995).

The turbulent velocity fluctuations of V_x, V_y and V_z all experienced maximum values shortly after the bore front passage. The peak of velocity fluctuations at vertical elevation close to the bed appeared earlier than at higher elevations close to the free surface. The largest velocity fluctuations were observed close to the bed. Tidal bore experiments in a horizontal channel by Leng and Chanson (2016) exhibited the same features. These features differed from those of stationary hydraulic jump experiments with Froude numbers larger than 3.1 by Chachereau and Chanson (2011), indicating that some longitudinal velocity fluctuations increase with increasing distance from the bed.

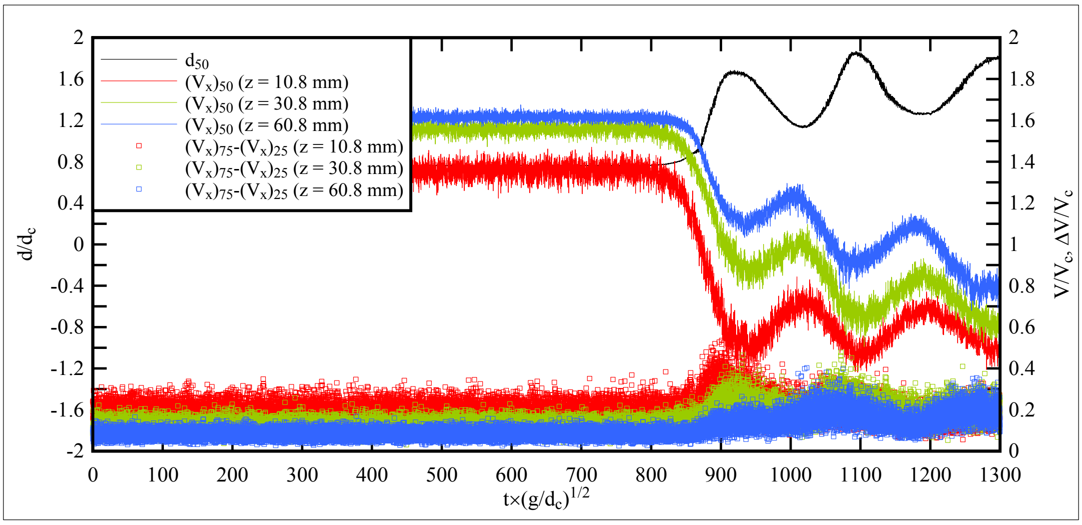

(A) Longitudinal velocity component.

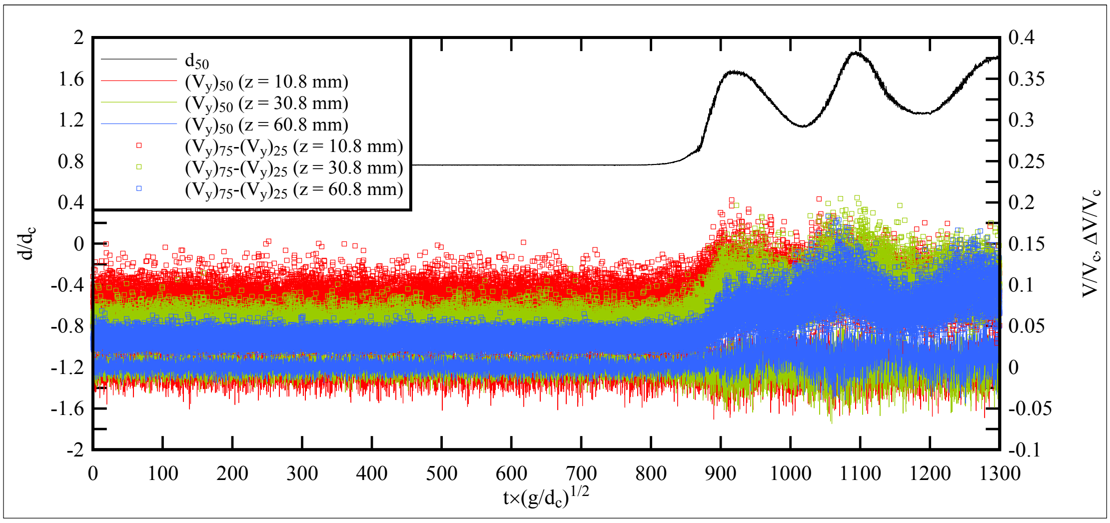

(B) Transverse velocity component.

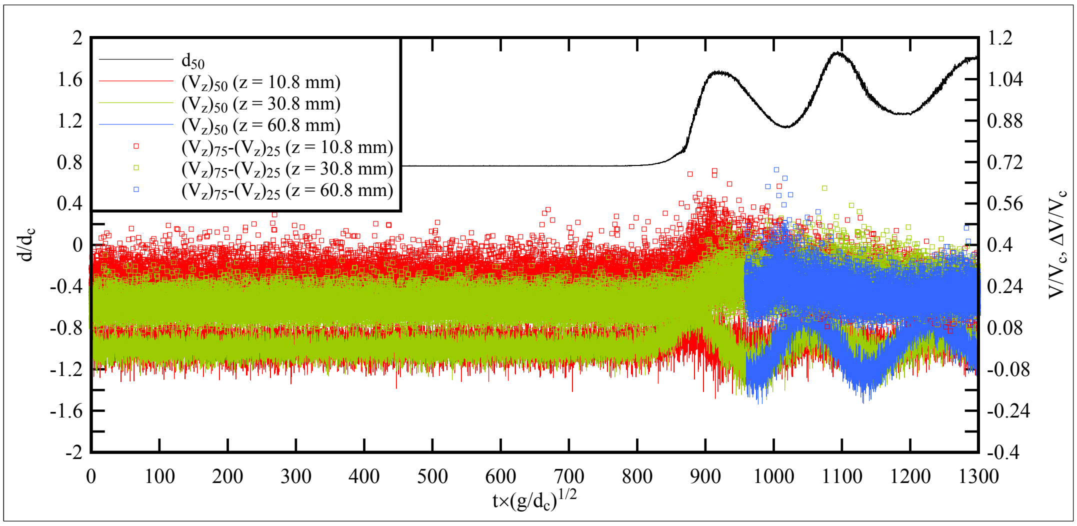

(C) Vertical velocity component.

Figure 6. Ensemble-averaged time variations of the median longitudinal, transverse and vertical velocity components and their velocity fluctuations (V_{75}-V_{25}) at different vertical elevations z for decelerating bores locally synchronized at x = 7.00 m - Flow condition: Q = 0.039 m^3/s, S_o = 0.0068, h = 0.080 m, Fr_1 = 1.52 at x = 7.00 m; d_c = 0.086 m, V_c = 0.9174 m/s.

5 CONCLUSIONS

The present work focused on the instantaneous and ensemble-averaged free-surface and velocity characteristics for decelerating bores against an adverse steep slope, and the transformation process of the travelling bore into a stationary hydraulic jump. For each flow condition, the experiment was repeated more than 25 times to enable ensemble-averaged measurements. The process of a decelerating bore and its transformation into an arrested bore was very slow, normally taking more than 300 s, compared to less than 20 s for a bore to travel through the entire horizontal channel. Both instantaneous free-surface measurements and ensemble-average analyses were conducted based on the data collected at six longitudinal locations. The shape of the decelerating bore gradually varied as it propagated upstream. The arrested bore could be an undular jump with long shock waves and strong secondary waves, a partially breaking jump with long shock waves and strong secondary waves, or a strongly breaking jump with short shock waves and weak secondary waves. The decelerating bore passage was observed with a marked rise in free-surface and some decrease of longitudinal velocity, as well as relatively large free-surface and velocity fluctuations. The time lag between maximum free-surface fluctuations and first wave crest increased with further distance from downstream gate. The bore front passage caused a significant rise in all the velocity components at all vertical elevations. At vertical elevations closer to the bed, the velocity fluctuations had an earlier response to the decelerating bore arrival and larger fluctuation amplitudes than at an upper elevation.

Overall, the present study presented seminal features of the slow and complicated process of decelerating bores with intense turbulence. The current experiment may be compared to in-situ tidal and tsunami bore process in estuarine zones. The varying characteristics of decelerating bores should be considered in the hydraulic structure designs in areas affected by tidal bores and tsunami bores.

ACKNOWLEDGEMENTS

The authors thank Ms Xinqian Leng, Mr Gangfu Zhang and Dr Hang Wang (The University of Queensland) for their assistance and advice. The technical assistance of Jason Van Der Gevel and Stewart Matthews (The University of Queensland) are acknowledged. The financial assistance of the Australian Research Council (ARC DP120100481) are acknowledged.

REFERENCES

Bellal, M., Spinewine, B., Savary, C. & Zech, Y. (2003). Morphological Evolution of Steep-Sloped River Beds in the Presence of a Hydraulic Jump: Experimental Study. *Proceeding 30th IAHR Biennial Congress*, Thessaloniki, Greece, C (2), 133-140.

British Standard (1943). *Flow Measurement*, British Standard Code BS 1042:1943, British Standard Institution, London.

Carling, P.A. (1995). Flow-Separation Berms Downstream of a Hydraulic Jump in a Bedrock Channel. *Geomorphology*, 11(3), 245-253.

Chachereau, Y. & Chanson, H. (2011). Bubbly Flow Measurements in Hydraulic Jumps with Small Inflow Froude Numbers. *International Journal of Multiphase Flow*, 37(6), 555-564.

Chanson, H. (2010). Unsteady Turbulence in Tidal Bores: Effects of Bed Roughness. *Journal of Waterway, Port, Coastal, and Ocean Engineering*, 136(5), 247-256.

Chanson, H. (2011a). *Tidal Bores, Aegir, Eagre, Mascaret, Pororoca: Theory and Observations*. World Scientific, 1-201.

Chanson, H. (2011b). Turbulent Shear Stresses in Hydraulic Jumps and Decelerating Surges: An Experimental Study. *Earth Surface Processes and Landforms*, 36(2), 180-189.

Chanson, H. (2012). Momentum Considerations in Hydraulic Jumps and Bores. *Journal of Irrigation and Drainage Engineering,* 138(4), 382-385.

Chanson, H. & Docherty, N.J. (2012). Turbulent Velocity Measurements in Open Channel Bores. *European Journal of Mechanics B/Fluids*, 32, 52-58.

Chanson, H. & Montes, J.S. (1995). Characteristics of Undular Hydraulic Jumps. Experimental Apparatus and Flow Patterns. *Journal of Hydraulic Engineering*, 121(2), 129-144.

Chanson, H., Reungoat, D., Simon, B. & Lubin, P. (2011). High-Frequency Turbulence and Suspended Sediment Concentration Measurements in the Garonne River Tidal Bore. *Estuarine Coastal and Shelf Science,* 95(2-3), 298-306.

Grant, G.E. (1997). Critical Flow Constrains Flow Hydraulics in Mobile-Bed Streams: a New Hypothesis. *Water Resources Research*, 33(2), 349-358.

Henderson, F.M. (1966). *Open Channel Flow*. MacMillan, 1-522.

Keevil, C.E., Chanson, H. & Reungoat, D. (2015). Fluid Flow and Sediment Entrainment in the Garonne River Bore and Tidal Bore Collision. *Earth Surface Processes and Landforms*, 40(12), 1574-1586.

Koch, C. & Chanson, H. (2008). Turbulent Mixing beneath an Undular Bore Front. *Journal of Coastal Research*, 24(4), 999-1007.

Koch, C. & Chanson, H. (2009). Turbulence Measurements in Positive Surges and Bores. *Journal of Hydraulic Research*, 47(1), 29-40.

Leng, X. & Chanson, H. (2015). Breaking Bore: Physical Observations of Roller Characteristics. *Mechanics Research Communications*, 65, 24-29.

Leng, X. & Chanson, H. (2016). Coupling between Free-surface Fluctuations, Velocity Fluctuations and Turbulent Reynolds Stresses during the Upstream Propagation of Positive Surges, Bores and Compression Waves. *Environmental Fluid Mechanics*, 16(4), 695-719.

Lennon, J.M. & Hill, D.F. (2006). Particle Image Velocimetry Measurements of Undular and Hydraulic Jumps. *Journal of Hydraulic Engineering*, 132(12), 1283-1294.

Liggett, J.A. (1994). *Fluid Mechanics*. McGraw-Hill, 1-495.

Lighthill, J. (1978). *Waves in Fluids*. Cambridge University Press, 1-504.

MacDonald, R.G., Alexander, J., Bacon, J.C. & Cooker, M.J. (2009). Flow Patterns, Sedimentation and Deposit Architecture under a Hydraulic Jump on a Non-Eroding Bed: Defining Hydraulic Jump Unit Bars. *Sedimentology*, 56, 1346-1367.

Parker, G. (1996). *Some speculations on the relation between Channel Morphology and Channel Scale Flow Structures. in Coherent Flow structures in Open Channels*. John Wiley, Chichester, UK, 423-458.

Parker, G. & Izumi, N. (2000). Purely Erosional Cyclic and Solitary Steps Created by Flow over a Cohesive Bed. *Journal of Fluid Mechanics*, 419, 203-238.

Treske, A. (1994). Undular Bores (Favre-Waves) in Open Channels - Experimental Studies. *Journal of Hydraulic Research*, 32(3), 355-370.

Yeow, S.C., Chanson, H. & Wang, H. (2016). Impact of a Large Cylindrical Roughness on Tidal Bore Propagation. *Canadian Journal of Civil Engineering*, 43(8), 724-734.

